AGU100 ADVANCING EARTH AND SPACE SCIENCE

Water Resources Research

TECHNICAL REPORTS: METHODS

10.1029/2018WR023420

Predicting Downstream Concentration Histories From Upstream Data in Column Experiments

Thomas Sherman[1], **Allan Foster**[2], **Diogo Bolster**[1], **and Kamini Singha**[2]

[1]Department of Civil and Environmental Engineering and Earth Sciences, University of Notre Dame, Notre Dame, IN, USA, [2]Hydrologic Science and Engineering, Colorado School of Mines, Golden, CO, USA

Key Points:
- We apply a fully parameterized spatial Markov model to predict breakthrough curves in zeolite clinoptilolite-packed column experiments
- Our experimental setup allows measurements of three breakthrough curves: two for model parameterization and one for validation
- Incorporating velocity correlation into the CTRW significantly improves BTC prediction for experiments run at Peclet numbers 121 and 1210

Correspondence to:
T. Sherman,
tsherma3@nd.edu

Citation:
Sherman, T., Foster, A., Bolster, D., & Singha, K. (2018). Predicting downstream concentration histories from upstream data in column experiments. *Water Resources Research*, *54*. https://doi.org/10.1029/2018WR023420

Received 8 JUN 2018
Accepted 30 SEP 2018
Accepted article online 11 OCT 2018

Abstract The scales of heterogeneity present in geologic media make modeling solute transport extremely challenging, even in idealized laboratory settings. The spatial Markov model (SMM) is an anomalous transport model that has been shown to accurately capture solute transport in a broad range of highly complex and heterogeneous hydrogeologic settings. However, to date, its applications are almost entirely limited to synthetic, numerically simulated systems due to the dense data required to parameterize it, which are typically unobtainable in real experiments. Here we apply a novel SMM inverse model that required only breakthrough curve measurements from laboratory transport experiments in zeolite-packed columns that are known to display anomalous transport. We introduce an experimental design that allows for simultaneous measurements of breakthrough curves at multiple sampling locations within a one-dimensional column setup. For the first time, we apply a fully parameterized SMM to successfully predict downgradient breakthrough curves. Results show that breakthrough curve prediction accuracy significantly improves when accounting for correlation effects in these experiments, a feature that the SMM is specifically designed to capture but that most traditional anomalous transport frameworks ignore. We do so for two different Péclet numbers, providing a parsimonious framework that can potentially account for correlation statistics in different field-scale studies.

1. Introduction

A variety of studies spanning several decades now show that solute transport in the subsurface displays behavior that is not consistent with predictions of classical models such as the advection-dispersion equation (Benson et al., 2000; Dentz & Berkowitz, 2003; Feehley et al., 2000; Goltz & Roberts, 1986; Haggerty & Gorelick, 1994; Harvey et al., 1994; Harvey & Gorelick, 2000; Major et al., 2011; Zinn & Harvey, 2003). Tracer experiments in field systems commonly show "anomalous," or non-Fickian transport, characterized by (1) early tracer breakthrough; (2) overestimated and underestimated mass recovery at early and late times, respectively; (3) tailing, or a gradual decrease in concentration through time, resulting in elevated concentration levels at late time; and (4) increased contaminant storage and rebound when compared to Fickian models. At the root of efforts to model transport in hydrologic systems accurately is the need to understand the processes and mechanisms that control anomalous solute transport. Processes that have been hypothesized to control this behavior, such as heterogeneous advection and local diffusion, are difficult to isolate using field-based approaches (e.g., pumping and tracer tests) alone (National Research Council, 2000). The parameters within existing anomalous solute transport models that control behavior are to date largely treated as fitting parameters, although some limited previous work has shown that these values may be correlated to the hydraulic conductivity field (Benson et al., 2001; Willmann et al., 2008), facies distributions (Zhang et al., 2007), and/or fracture length scale (Reeves et al., 2008). The main limitation of many nonlocal models is the weak predictability of the model and its main parameters (Zhang et al., 2009); in other words, the physical meaning of many of the parameters within the models is difficult to measure or correlate conclusively to geology (Willmann et al., 2008). For example, it has been observed that systems with identical statistical length scales exhibit quite different solute behavior, suggesting pathway connectivity is an important parameter to consider. Unfortunately, no reliable measure of in situ connectivity exists. While it has been suggested that tracer paths can be used as a metric for connectivity, quantifying pathways in natural systems has proven difficult given the limited data collected during standard tracer tests. Further, a limited number of well-controlled experiments have been conducted exploring the physical meaning of the fitted parameters. If we are looking for predictive abilities in such systems, it is critical to work with adequate frameworks that capture this anomalous behavior.

Part of the state of the art for modeling solute transport is continuous time random walks (CTRWs), which conceptualize a solute plume as a finite number of discrete particles. At each model step particles transition in space and time by probabilistically sampling a waiting time and jump distance from a given distribution. Traditionally, independence is assumed between successive particle jumps. However, this assumption has been shown to be violated in a multitude of studies (Bolster et al., 2014; de Anna et al., 2013; Le Borgne et al., 2008a; Morales et al., 2017; Sund et al., 2015). The spatial Markov model (SMM) accounts for velocity correlation between particle jumps and has proven particularly advantageous when predicting transport in systems displaying intermittent behavior (de Anna et al., 2013; Kang et al., 2014). The SMM captures intermittency generated from microscale features in an upscaled framework, equipping it to accurately portray larger-scale transport. It has been successful in modeling transport across a diverse range of synthetic systems of interest, including flows through highly heterogeneous permeability fields (Le Borgne et al., 2008b, 2008a), complex pore-scale systems (Kang et al., 2014), inertially dominated systems (Bolster et al., 2014; Sund et al., 2015), and fractured media (Kang et al., 2011, 2015, 2016). Recently, it was also extended to predict reactive transport (Sund et al., 2016; Sund, Porta, Bolster, & Parashar, 2017) as well as mixing and dilution effects (Sund, Porta, & Bolster, 2017).

In the vast majority of the SMM literature, the correlation structure is found by tracking a very large number of particle trajectories in high-resolution numerical simulations and explicitly calculating corresponding statistics (Le Borgne et al., 2011; Sund et al., 2016). However, using such particle tracking methods in real systems is completely unfeasible. In most practical contexts the best one might hope for is breakthrough curves at multiple downstream locations, from which such information is difficult to tease out. Therefore, the SMM's applicability to laboratory and field studies has been limited, with one notable exception (Kang et al., 2015), who apply the SMM to nonsynthetic data, but assume a simplified correlation structure and fit an additional parameter to field-scale push-pull fractured experimental data. The brilliance of this simplification is that it dissolves the SMM's reliance on Lagrangian statistics. This is currently the best attempt at applying the SMM to a real system but is potentially limiting as the assumed structure may not reflect universal behaviors and there is still no generalized method to best estimate the SMM's correlation in real-world settings.

Sherman et al. (2017) introduced an inverse SMM model to estimate velocity correlations using data from breakthrough curves alone. This algorithm was shown to accurately predict transport in highly idealized numerical systems but remains untested on observed data. Here, for the first time, we apply the SMM inverse algorithm to real data that display anomalous behavior. We collect data from columns packed with the zeolite clinoptilolite, a material that demonstrates non-Fickian transport due to a substantial intragranular porosity consisting of a distribution of pore sizes (Kowalczyk et al., 2006; Sprynskyy et al., 2010). We believe such complexity gives rise to intermittent behavior and therefore expect the SMM to be more capable than other models in accurately predicting the transport observed in these experiments. It has been difficult to characterize this complexity, even in columns, such that we can predict transport phenomena (Swanson et al., 2012, 2015). For these experiments, we inject a finite-volume pulse of conservative NaCl tracer at the column inlet and measure breakthrough curves at three downgradient sampling ports, enabling characterization of the temporal and spatial evolution of the solute plume. We use observations from the first two sampling ports to accurately predict breakthrough time evolution downgradient, all under a parsimonious mathematical framework. The inverse SMM's robustness is tested by running experiments with Péclet numbers equal to 121 and 1210.

2. Methods

Laboratory tracer experiments were conducted using a conservative NaCl tracer pushed upward through a zeolite clinoptilolite medium. The experimental column was 124.5 cm in length, 5.2 cm in diameter, and was made from clear PVC with multiple equally spaced sampling ports positioned 20.8, 41.6, 62.4, 83.2, and 104.0 cm from the column's inlet. This allowed simultaneous collection of fluid electrical conductivity measurements at desired locations within the system (Figure 1). Breakthrough curves from sampling ports positioned at L/6 and 2L/6, where L is the column length, are used as inputs for the SMM inverse framework. Measurements at sampling port 5L/6 allowed for predictions from the SMM to be compared with observed experimental measurements. From here on, sampling ports L/6, 2L/6, and 5L/6 will be referred to as sampling ports 1,2, and 5, respectively, and corresponding data BTC 1, BTC 2, and BTC 5. A schematic of the column design and the process of how observed data are input into the SMM is provided in Figure 1.

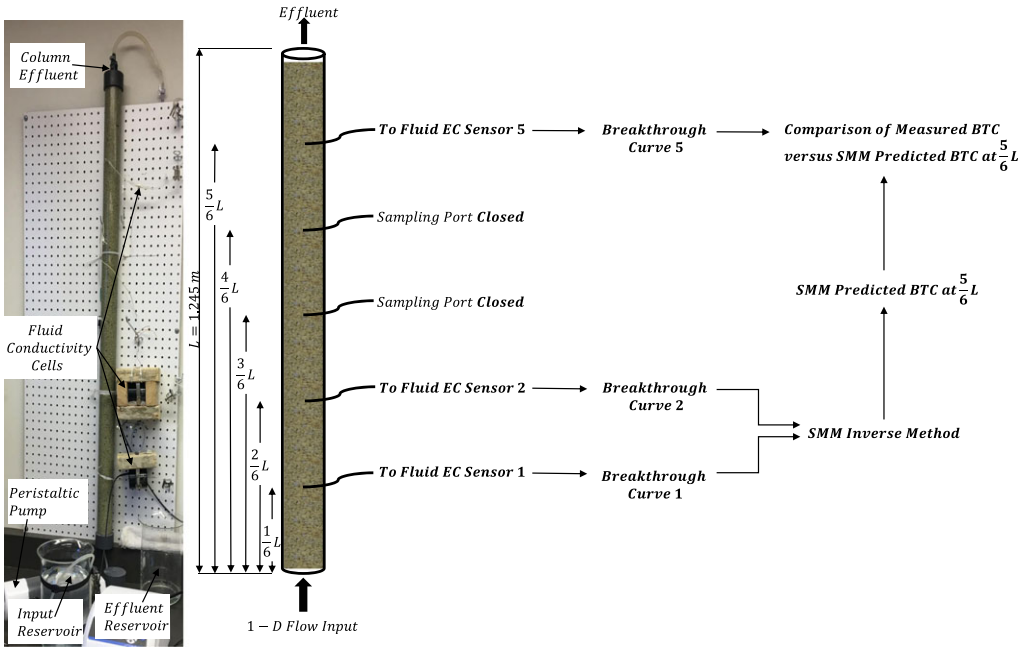

Figure 1. Conceptual model of laboratory-produced data pathway for input into the SMM framework. SMM = spatial Markov model; BTC = breakthrough curve; EC = electrical conductivity.

2.1. Material Characterization, Solution, and Fluid Electrical Conductivity Sensor Preparation

The material utilized in these experiments consisted of a zeolite clinoptilolite, which has coarse, angular grains. The distribution of grain and intragranular pore size within the column creates a complex intergranular and intragranular pore space, representative of complexity in natural systems.

Porosity ranges for this zeolite are characterized in Swanson et al. (2012) and Swanson et al. (2015) and sieve analyses (Table 1). The zeolite was composed of 69.1% SiO_2, 11.9% Al_2O_3, 3.8% K_2O, and 3.5% Na_2O, with trace

Table 1
Experimental Specifications and Pe Calculation Values

Parameter	Detail
Internal column diameter (cm)	5.2
Column length (cm)	124.5
Grain size range (cm)	0.2–0.48
D_{10} (cm)	0.22
D_{50} (cm)	0.3
D_{60} (cm)	0.32
Assumed characteristic length, l (average grain diameter) (cm)	0.31
Intergranular porosity (–)	0.46
Intragranular porosity (–)	0.20
Diffusion coefficient of Na in open water, D^* (cm^2/s)	0.000013
Total flow rates (cm^3/s)	0.083, 0.83
Internal sampling port diameter (cm)	0.16
Sampling port flow rate (cm^3/s)	0.0034, 0.017
Tortuosity, ω (–)	1.6
Average linear velocity, v (cm/s)	0.0081, 0.081
Pe (–)	121, 1210
Temperature (°C)	23

amounts of Fe_2O_3, TiO_2, CaO, MgO, and MnO (St. Cloud Mining, 2013). The zeolite was saturated in deionized (DI) water and stirred until all possible air was replaced with water.

The tracer and background concentrations were 0.45 and 0.074 g/L NaCl. The tracer solutions were made with degassed DI water from a Millipore purifier, thoroughly mixed, and stored in airtight high-density polyethylene storage containers.

The fluid conductivity sensors utilized in the experiments consisted of two micro-flowthrough Amber Scientific sensors with a sampling volume of 7 μL and measurement resolution of ±0.01μS/cm at sampling ports 1 and 2. A Microelectrodes micro-flowthrough conductivity cell with a sampling volume of 25 μL and measurement resolution of ±0.1μS/cm was used at sampling port 5. The cells were each calibrated using three calibration solutions consisting of 1,413, 2,764, and 12,880 μS/cm at a temperature of 23 °C. The sensors were calibrated prior to every experimental run.

2.2. Column Packing

Columns were wet packed using preprepared, fully saturated zeolite clinoptilolite grains to minimize air being trapped between grains. Wet packing involved filling the column (empty) from the bottom to the top with DI water using a Cole-Parmer peristaltic pump at a low flow rate (10 ml/min or less) while gently tapping the side of the column endcap with a rubber mallet to force air trapped in the end cap out of the system. Once the column was partially full of DI water, the pump was stopped. Then zeolite grains were incrementally added to the column from their saturation container in 1-cm increments, as was done in previous similar column experiments with zeolite grains (Briggs et al., 2014; Swanson et al., 2012, 2015). Tapping allows grains to settle into a uniformly distributed packing. Once completely filled with zeolite, the top endcap was attached and the peristaltic pump was turned on to push any trapped air out the top endcap. Next, the column was flipped 180° (upside down). In preliminary experiments where the column was not flipped, the average linear velocity between sampling ports as the tracer transported vertically through the column showed an increasing flow rate through the medium due to an unevenness in packing, despite best efforts otherwise. Flipping the column prior to starting the tracer experiments effectively mitigated the unevenness in average linear velocity between sampling ports.

2.3. Experimental Procedure and Péclet Number Formulation

The experimental procedure consisted of first flushing the packed column with degassed DI water until the material was "clean," as determined by observation of the effluent from the top of the column. Once clean, the background solution was injected and sampling ports 1, 2, and 5 were opened and controlled such that port flow rates were equal and their cumulative discharge was approximately 10% of the total flow rate, maintaining the 1-D flow assumption (Briggs et al., 2014). Each sampling port had a flow-rate control clamp to keep a constant sampling flow rate throughout the full duration of the tracer test.

The column flow rates used in the tracer tests were 5 and 50 mL/min. This corresponded with Péclet numbers *Pe* varying an order of magnitude from approximately 121 to 1210. The lower *Pe* case was chosen in order to test the SMM with experimental flow conditions representative of natural groundwater systems. The higher *Pe* case corresponds to a regime in which significant velocity correlation is expected and consistent with past numerical studies (Bolster et al., 2014). The *Pe* analysis of these experiments is derived from Freeze and Cherry (1979) with a diffusion coefficient from Yuan-Hui and Gregory (1974) but modified for tortuosity as referenced in Huysmans and Dassargues (2005) using an empirically derived relationship between porosity of a medium and tortuosity developed in Matyka et al. (2008):

$$Pe = \frac{vl}{\omega D^*} \tag{1}$$

where v is the average linear velocity in the vertical direction, l is the average grain diameter, D^* is diffusion coefficient of Na^+, and ω is the tortuosity.

Once the fluid conductivity at each of the three sampling ports reached pseudo-equilibrium conditions (fluid conductivity changes of less than ±1μS/cm around the conductivity of the background solution), the tracer solution was injected as a finite volume pulse of 66 mL. This was performed by changing the input reservoir for a determined time at the experimental flow rate; this required 790 or 79 s of injection for the lower and higher *Pe* cases, respectively. After the tracer pulse injection, the input reservoir was immediately switched back to injecting the background solution. Fluid conductivity was simultaneously recorded at a minimum 1-min temporal resolution for all three sensors during tracer breakthrough. An experiment was concluded

when fluid conductivity values for each of the three sensors read the same fluid electrical conductivity value as prior to tracer pulse injection and did not change more than ±1μS/cm. Once completed, experimental data were processed and fed into the SMM framework. Table 1 summarizes necessary experimental information.

3. Modeling: SMM and Inverse Algorithm

3.1. The SMM

In the SMM, a solute plume is discretized into N particles, with N sufficiently large. We use $N = 5 \times 10^5$ in this study. Each particle's trajectory through time and space is governed by the Langevin equation

$$x_i^{n+1} = x_i^n + L_c \tag{2}$$

$$t_i^{n+1} = t_i^n + \tau_i^n \tag{3}$$

where during the nth model iteration, particle i jumps a fixed distance of L_c with a travel time τ_i^n randomly sampled from a distribution $\psi(\tau)$. In other words, our domain is divided into cells of distance L_c and at each model step, the SMM characterizes the time it takes to travel one cell. The time for particle i to reach the outlet of the nth cell is the summation of travel times, $t_i^n = \sum_{j=1}^{n} \tau_i^j$. The SMM assumes velocity statistics are stationary over each cell (Sund et al., 2015), which implies that the travel-time distributions for all cells are identical. We choose a sufficiently large cell length, L_c, to satisfy this assumption. In this study $L_c = 20.8$cm, which is 1/6th the column length, L.

A key feature of the SMM is that successive travel times can be correlated, relaxing the assumption of independence inherent to many random walk models. These correlations reflect an underlying behavior that particles that make a fast/slow transition across one element may often make a fast/slow transition across the next one also, which has been shown to be the case in high-Pe number systems, when advective processes dominate diffusion. Specifically, Bolster et al. (2014) showed correlation should be considered when $Pe > O(100)$. In our column experiments we test at $Pe \sim O(100)$ and $O(1000)$.

The SMM accounts for such correlations through a transition matrix. We divide the travel-time distribution into k classes of equal probability, such that class 1 contains the fastest travel times and class k contains the slowest. The transition matrix T is then of size $k \times k$. The value of element $T_{i,j}$ is the probability a particle has a travel time in class j at the $n + 1$ model step, given it had a travel time in class i at model step n:

$$T_{i,j} = P(\tau^{n+1} \in class\, j | \tau^n \in class\, i) \tag{4}$$

In this study, we choose $k = 25$, which is sufficient to capture correlation effects. For more details on implementation, see Le Borgne et al. (2011) and Bolster et al. (2014).

3.2. Inverse SMM Algorithm

Sherman et al. (2017) introduced an inverse algorithm to estimate the SMM's transition matrix using breakthrough curve data alone. Specifically, given that a solute is released at $x = 0$, the inverse algorithm requires breakthrough measurements at two locations $x = L_c$ and $2L_c$, referred to as $BTC1$ and $BTC2$, respectively.

Consistent with the SMM theory, we assume the travel-time distributions for each cell in the column are stationary. Then $BTC1$, appropriately normalized, approximates each cell's travel-time distribution. Discretizing $BTC1$ into M travel times enables us to estimate the probability of the mth travel time

$$P(\tau_m) = \frac{A_m}{\sum_{h=1}^{M} A_h}. \tag{5}$$

A_m is the area under $BTC1$ in the interval $[\frac{1}{2}(\tau_m - \tau_{m-1}), \frac{1}{2}(\tau_{m+1} - \tau_m)]$. Similarly, a discrete distribution can be constructed for $BTC2$. Here $BTC1$ and $BTC2$ were discretized into equally spaced time intervals of 0.1 min. We denote these as $PDF1$ and $PDF2$.

This discretization provides enough information to estimate the transition matrix for the system. Let $\tilde{\tau}_2^z$ be the vector of arrival times for $x = 2L_c$, that is, the discretized times for $BTC2$. Let $\tilde{\tau}_1^a$ be the vector of arrival times for $BTC1$ and $\tilde{\tau}_1^b$ be the vector of times to travel from $x = L_c$ to $x = 2L_c$. The stationarity assumption requires that $\tilde{\tau}_1^a$ and $\tilde{\tau}_1^b$ follow the same distribution. The discretized governing equation for the SMM follows:

$$P(\tilde{\tau}_2^z) = \sum_{\tilde{\tau}_1^a + \tilde{\tau}_1^b = \tilde{\tau}_2^z} P(cell1 = \tilde{\tau}_1^a) P(cell2 = \tilde{\tau_1}^b | cell1 = \tilde{\tau}_1^a) \tag{6}$$

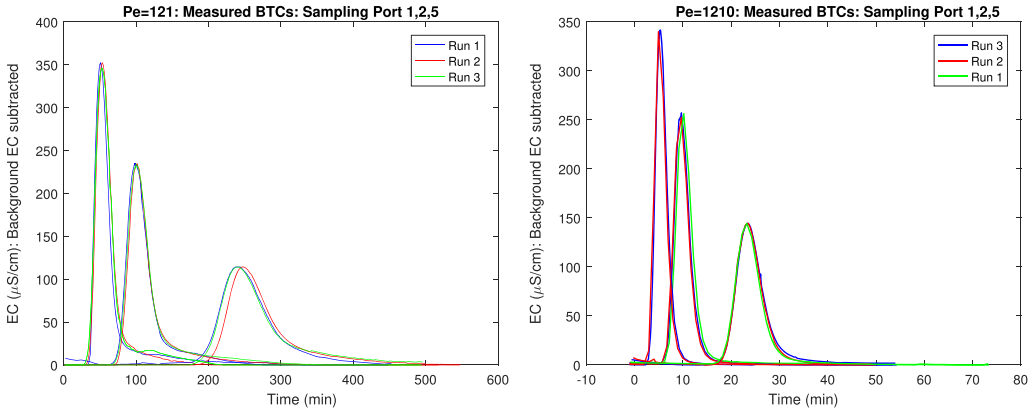

Figure 2. Experimental data of breakthrough curves measured at sampling ports 1,2, and 5 for each of three repeat runs. Sampling ports are positioned at approximately 0.21, 0.42, and 1.04 m from the column inlet, which correspond to 1/6, 2/6, and 5/6 the total column length, respectively. Background conductivity is subtracted from each curve. BTC = breakthrough curve; EC = electrical conductivity.

Equation (6) states the probability of arriving at the outlet of the second cell in time τ_2^z is the summation of all probabilities of choosing two successive travel times that sum to τ_2^z. If we divide *BTC*1 into *k* bins, where bin 1,*k* contains the fastest, slowest arrival times, we can write an equation statistically equivalent to (6):

$$P(\tilde{\tau}_2^z) = \sum_i \sum_j \underset{\tilde{\tau}_1^a + \tilde{\tau}_1^b = \tilde{\tau}_2^z}{} P(cell1 = \tilde{\tau}_1^a, bin\ i) T_{i,j} P(cell2 = \tilde{\tau}_1^b | bin\ j) \tag{7}$$

In words, the probability of a τ_2^z arrival time at $x = 2L_c$ is the probability of all combinations of successive travel times that sum to τ_2^z. For τ_1^a in bin *i* and τ_1^b in bin *j*, the probability of this combination is the product of the probability of choosing τ_1^a, the probability of transitioning from bin *i* to bin *j*, and the conditional probability of choosing a τ_1^b arrival time in bin *j*. *PDF*1 gives a cell's travel-time distribution, and *PDF*2 gives the cell 2 arrival-time distribution, so we can write a system of equations to find each $T_{i,j}$, the elements in the transition matrix. For τ_2^q, the *q*th element in $\tilde{\tau}_2^z$, we solve

$$P(\tau_2^q) = (p_{q,(1,1)} \cdots p_{q,(k,k)}) \times \begin{pmatrix} T_{1,1} \\ \vdots \\ T_{k,k} \end{pmatrix} \tag{8}$$

Note that we create a matrix of size $q \times k^2$ using (8). Element $p_{q,(i,j)} = \sum_{\tau_1^a + \tau_1^b = \tau_2^q} P(cell1 = \tau_1^a, bin\ i) P(cell2 = \tau_1^b | bin\ j)$, acts as a weight for each *T* element in the equation. In this system of equations there exists k^2 unknowns and *Q* known values, where *Q* is the length of the $\tilde{\tau}_2^z$ vector. If $Q \geq k^2$, we can solve the system and estimate the transition matrix. The discrete, approximate nature of this process leads to a transition matrix that can closely approximate actual values as shown in the synthetic examples of Sherman et al. (2017), but some natural uncertainty and variability means that an additional level of filtering can help to improve matches between BTC1 and BTC2. In this study, we observed overestimates of concentration at late times for BTC2. This was corrected by artificially lowering the transition probabilities into slow time bins until predicted BTCs more accurately captured late time tailing behavior (Figure 3). For full details on the implementation of the inverse SMM as well as a sample code see Sherman et al. (2017) and Sherman (2018).

4. Results and Discussion

The experimental setup measures BTC1 and BTC2, which enables prediction of BTCs downgradient via application of the inverse SMM algorithm. The measured BTC at sampling port 5 allows comparison between observed measurements and predictions. To demonstrate the strength of our procedure, we apply two predictive models: (i) the SMM as described above using our estimated transition matrix and (ii) an uncorrelated CTRW, which also follows Langevin equation (2), but where no correlation is imposed on successive jumps (equivalent to a completely uniform transition matrix).

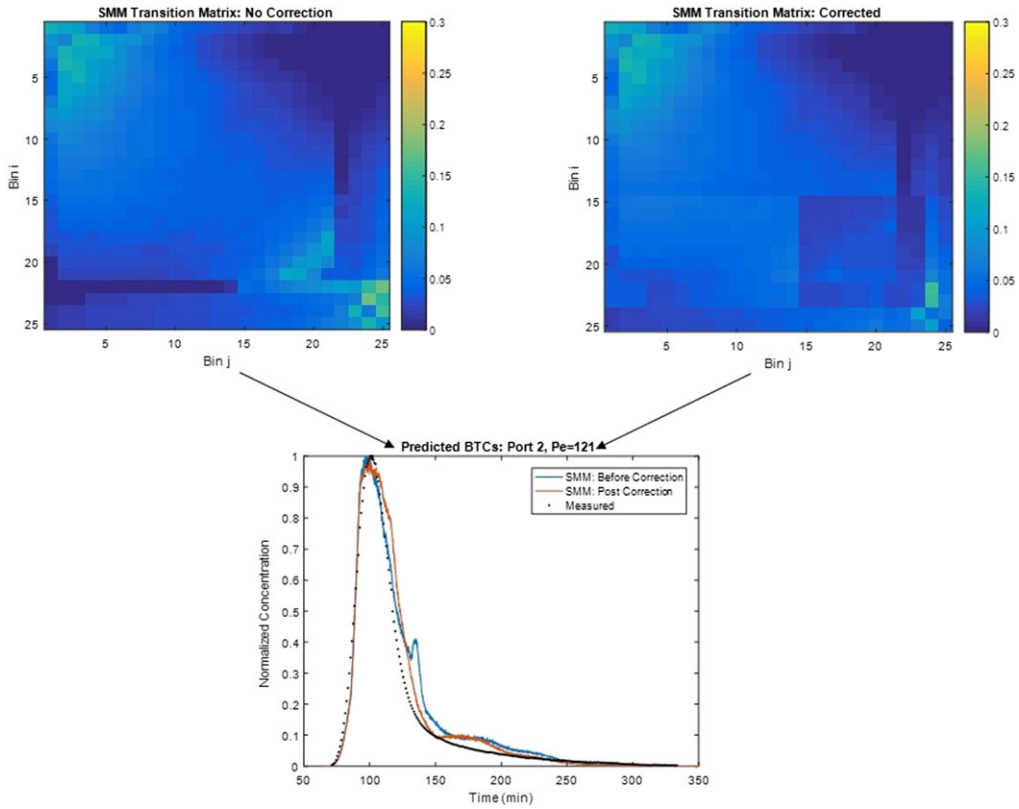

Figure 3. Shown is an example of the correction process for run 2 of the *Pe* = 121 case. The top left transition matrix has no correction. It predicts a strong kink near 150 min and overestimates late tailing behavior at port 2. In the corrected matrix (top right), the values for transitioning into bin 25 are artificially lowered, slightly lowering late time prediction. Additionally, we lower the strongly correlated structure that is causing the kink. This small correction improves predictions at *BTC*5 (Figure 4). BTC = breakthrough curve; SMM = spatial Markov model.

All experiments were conducted in triplicate. The $Pe = 1210$ runs display a high degree of reproducibility, which is also seen at $Pe = 121$, but with a little more variability (Figure 2), as lower flow rates in these experiments are more sensitive to any fluctuations at the ports, enhancing relative noise at late times when the difference between solute and background concentration is low. Note in the $Pe = 1210$ case, an instrumentation error at port 1 prevented measurement of a BTC in run 1, but given the high degree of reproducibility between experiments, this was deemed unimportant.

After subtracting off the background conductivity, we discretize BTC1 and BTC2 into a finite set of times and estimate the transition matrix for each run by applying the SMM inverse algorithm. At both *Pe* numbers, transition matrices exhibit diagonal trending (from top left to bottom right of the matrices), indicating the velocity correlation is significant (Figure 4). As expected, the $Pe = 1210$ transition matrix exhibits a stronger correlation, demonstrated by higher values in upper left and lower right corners. Physically, the diagonal trending suggests that fast channels, carved through the pore space between the zeolites, exist. Solute particles preferentially enter and remain in these channels as they transport through the column. The slowest travel times are likely induced by solute being trapped within the intragranular porosity. The upper right corner of both matrices has probabilities near zero, meaning solute in fast channels in one cell will most likely not experience these trapping mechanisms in the subsequent cell. In general, the predicted transport by the transition matrix is consistent with the column's geologic characteristics.

Due to noise and possibly resolution of experimental measurements, the proposed inverse SMM model is not perfect and so we treat the SMM inverse-estimated transition matrix as a "first-guess," and then tune it to better fit experimental data (Figure 3). Staying true to the philosophy of the model, we only use data from BTC1 and BTC2 in this process. Tuning the transition matrix involves predicting BTC2 using the first-guess matrix and BTC1 as an input. Note that this tuning procedure is only applied to bins that exhibit obvious

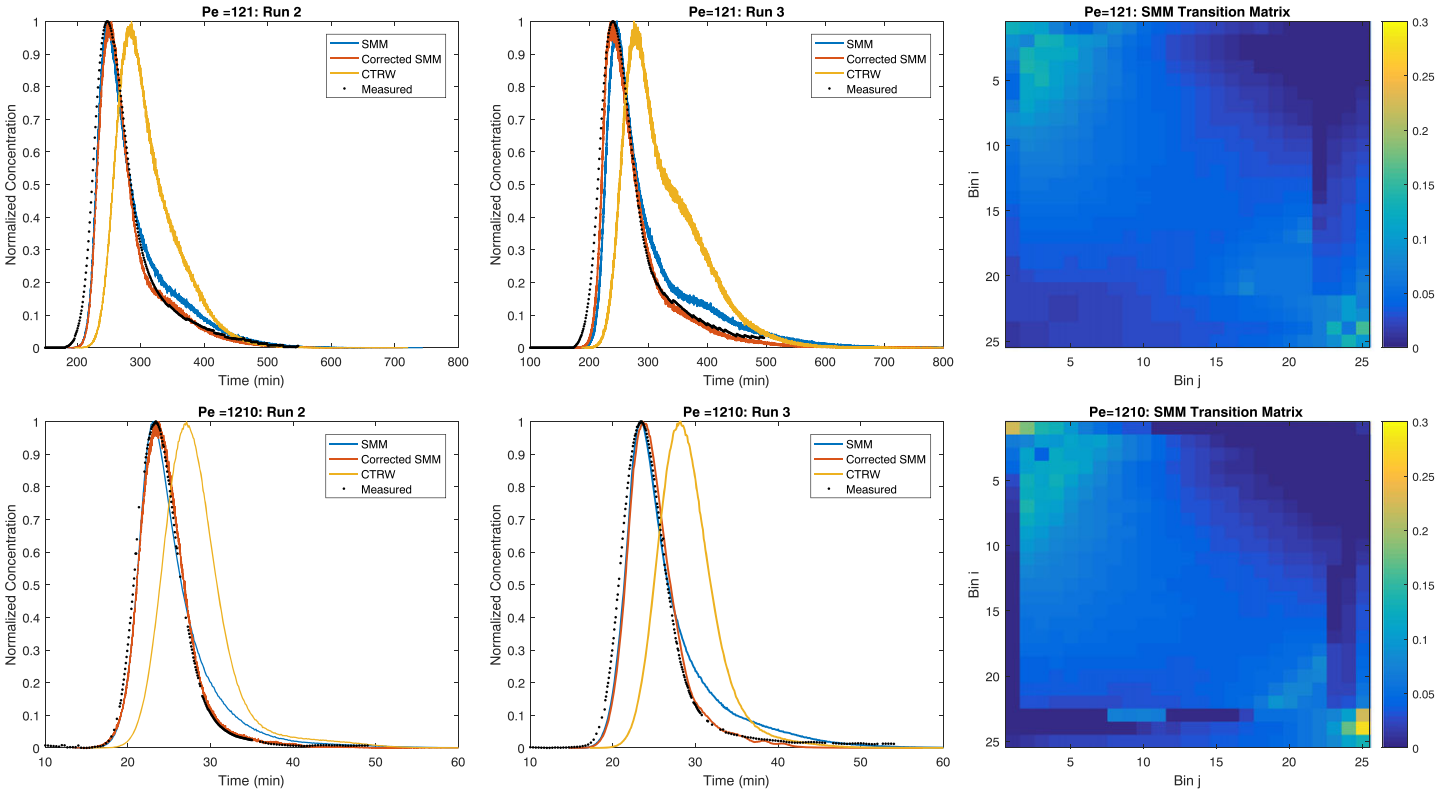

Figure 4. A comparison between experimental observations at sampling port 5 with predictions made using an uncorrelated CTRW, a parameterized SMM with no tuning applied, and a SMM where the transition matrix was corrected using *BTC*2 data. Experiments were run at *Pe* = 121, 1210. The representative estimated transition matrices for each *Pe* case are shown. Matrices varied slightly run by run but were very similar for each *Pe* number. SMM = spatial Markov model; BTC = breakthrough curve; CTRW = continuous time random walk.

experimental artifacts and no information from *BTC*5 is ever used in this process. The tuning procedure requires the following steps:

1. Apply the inverse SMM to estimate the transition matrix and predict *BTC*2.
2. Compare the predicted and measured *BTC*2 and inspect that early and late times match, as these regions are most difficult to predict accurately. Also inspect for any significant deviations in the predicted BTC. Note in this study we rely on visual inspection, but one could define an error threshold to identify spots where the predicted BTC needs correction.
3. Artificially adjust the estimated transition matrix elements that cause BTC predictions to fail. After "error" bins are tuned, we normalize rows to ensure the cumulative row probability is unity. In this work we normalize by dividing each element by the cumulative row probability. Note that the top left and bottom right portion of the matrix controls early and late time arrival, respectively. Furthermore, in our experience, unusual predicted BTC behavior corresponds to estimated transition matrix bins that are clearly wrong, that is, significantly higher or lower than neighboring bins. In this study, we identified error bins by visual inspection. A possible algorithmic solution would be to define a threshold and ensure that the difference between neighboring bins within a row does not exceed that threshold. Transition matrix rows in many systems lie on a smooth spectrum and such jumps in probability between bins is not typically observed.
4. Predict *BTC*2 with the tuned transition matrix and repeat steps 2 and 3, until the predicted *BTC*2 satisfies set error requirements.

Figure 3 provides an example of the tuning process for $Pe = 121$ on run 2. The predicted *BTC*2 using the first-guess transition matrix overestimated late time tailing. To correct this problem we divide the bins controlling late-time tailing ($T_{23,23}...T_{25,25}$) by a constant factor (approximately 2) and then normalized the rows such that they sum to 1. Additionally, an unusual kink appeared in the first-guess *BTC*2 prediction at a time of approximately 140 min. This kink is produced by the unusually high estimated matrix elements near $T_{20,20}$, which appear as a brightly colored bend. Again, we divide these elements by a constant factor and normal-

ize. We rerun the SMM with the tuned matrix and the kink lessens in the *BTC*2 prediction. The tuned transition matrix is then used to predict *BTC*5. By manually adjusting the bins causing the kink, we significantly improved predictive capability. While this tuning method is not algorithmic, a number of optimization metrics could be used to determine a "best" fit. However, given small corrections can easily be found by visual inspection, no such automated optimization procedure was implemented here. The purpose of manually tuning the estimated transition matrix is to demonstrate that the estimated matrix can be improved and only minor adjustments must be made to achieve accurate predictions. However, even without the tuning process the inverse SMM method still captures general velocity correlation trends and therefore significantly improves upon an uncorrelated CTRW. Estimated and tuned transition matrices from this experiment are made public via Github so that results may readily be reproduced by the community at large (see the acknowledgments section for details).

With this we can now run three predictions (uncorrelated CTRW, SMM with first-guess matrix, and SMM with tuned matrix) for BTCs at port 5 and compare with experimental observations. In all runs, the tuned SMM outperforms the uncorrelated CTRW and accurately predicts early, peak, and late-time concentration arrivals (Figure 4). The SMM predictions without tuning capture peak concentration arrival but overestimate late-time tails. In all runs, the noisiest measurements occur at late times, as there is challenge in distinguishing between low solute concentration and the background solution. Model inputs therefore contain this noise, which propagate and appear in predictions. Additionally, fluctuations in sampling port rates can generate error. However, despite these limitations the "tuned" SMM predicts BTCs remarkably well and even the first-guess SMM offers a significant improvement upon the uncorrelated CTRW model. Given this success we believe that the SMM, coupled with our novel inverse model, is ready for testing and application to field-scale systems.

Like other upscaled models, the SMM is a representative elementary volume approach, meaning the model is only valid and applicable at field-scale sites where the assumptions of representative elementary volume theory holds; that is, model parameters are stationary across elementary volumes. The SMM has been shown to accurately predict simulated transport in heterogenous 3-D porous media generated from real geologic samples (Kang et al., 2014), and so we expect our inverse algorithm to perform well for similar representative field sites. The quasi-one-dimensional design of the experimental columns means all solute sampled at the initial two ports is transported to the third port. In higher dimensional flows, it is possible that solute is transported in the transverse direction and thus never reaches the downstream sampling port. This is a well-known challenge, faced, for example, in the well-known Macrodispersion Experiment site experiments where mass recovery rates appeared very low (e.g., Harvey & Gorelick, 2000). Such challenges plague application of any upscaled transport models to real field conditions, and overcoming those specific hurdles is a challenge to be met by the community at large. However, if SMM parameters exhibit stationarity along the direction of flow and integrated concentration breakthrough curves can be reliably measured downstream, then our approach should be applicable for predicting large-scale downstream transport. Should mass loss occur, but also meet the stationarity requirement in terms of percent mass loss, then this could likely be accounted for by introducing a limbo state as was done by Sund et al. (2015). If such conditions are not met then the SMM may not be an appropriate model and an alternative approach should be sought.

5. Conclusions

For the first time, we predict BTCs associated with tracer tests at downgradient locations based on two curves from upgradient locations using a fully parameterized SMM. This work is an important step to predicting transport in complex heterogeneous field systems. Even in these idealized 1-D columns, the influence of small-scale geologic heterogeneity cannot be overlooked as small-scale effects alter BTC evolution just 1 m from the solute source. These heterogeneity effects would continue to propagate downgradient in a larger system, causing further deviation from predictions in traditional models. The effectiveness of the SMM is that it statistically incorporates small-scale correlation effects into its framework and therefore can accurately predict anomalous transport in complex environments. Although BTC predictions using our inverse method are not perfect, they offer a significant improvement upon current state-of-the-art models and provide an excellent first guess at the transition matrix, which can be further optimized quite easily given two breakthrough histories. Predicting anomalous behavior is of great importance for a number of field systems, including groundwater remediation (Harvey et al., 1994) and aquifer storage and recovery operations (Culkin et al., 2008). Therefore, if we hope to accurately predict transport in such systems, our models must accurately account for small-scale physical processes that control large-scale emergent behaviors, as the SMM does.

Acknowledgments
The code used to test our theoretical framework and experimental data is made public at https://github:com/tjsherman24/SMM-Inverse-Model. The authors would like to thank NSF for financial support for this work. This material is based upon work supported by, or in part by, NSF grants EAR-1351625, EAR-1417264, and EAR-1446236.

References

Benson, D. A., Schumer, R., Meerschaert, M. M., & Wheatcraft, S. W. (2001). Fractional dispersion, Lévy motion, and the made tracer tests, *Dispersion in heterogeneous geological formations* (pp. 211–240). Netherlands: Springer.

Benson, D. A., Wheatcraft, S. W., & Meerschaert, M. M. (2000). Application of a fractional advection-dispersion equation. *Water Resources Research*, *36*(6), 1403–1412.

Bolster, D., Méheust, Y., Borgne, T. L., Bouquain, J., & Davy, P. (2014). Modeling preasymptotic transport in flows with significant inertial and trapping effects—The importance of velocity correlations and a spatial Markov model. *Advances in Water Resources*, *70*, 89–103.

Briggs, M. A., Lewis, F. D. D., Ong, J. B., Harvey, J. W., & Lane, J. W. (2014). Dual-domain mass-transfer parameters from electrical hysteresis: Theory and analytical approach applied to laboratory, synthetic streambed, and groundwater experiments. *Water Resources Research*, *50*, 8281–8299. https://doi.org/10.1002/2014WR015880

Culkin, S. L., Singha, K., & Day-Lewis, F. D. (2008). Implications of rate-limited mass transfer for aquifer storage and recovery. *Groundwater*, *46*(4), 591–605. https://doi.org/10.1111/j.1745-6584.2008.00435.x

de Anna, P., Le Borgne, T., Dentz, M., Tartakovsky, A. M., Bolster, D., & Davy, P. (2013). Flow intermittency, dispersion, and correlated continuous time random walks in porous media. *Physical Review Letters*, *110*(18), 184502.

Dentz, M., & Berkowitz, B. (2003). Transport behavior of a passive solute in continuous time random walks and multirate mass transfer. *Water Resources Research*, *39*(5), 1111. https://doi.org/10.1029/2001WR001163

Feehley, C. E., Zheng, C., & Molz, F. J. (2000). A dual-domain mass transfer approach for modeling solute transport in heterogeneous aquifers: Application to the Macrodispersion Experiment (MADE) site. *Water Resources Research*, *36*(9), 2501–2515. https://doi.org/10.1029/2000WR900148

Freeze, R., & Cherry, J. (1979). *Groundwater Englewood Cliffs*. New Jersey: Prentice Hall.

Goltz, M. N., & Roberts, P. V. (1986). Interpreting organic solute transport data from a field experiment using physical nonequilibrium models. *Journal of Contaminant Hydrology*, *1*(1), 77–93. https://doi.org/10.1016/0169-7722(86)90008-2, transport and Transformations of Organic Contaminants.

Haggerty, R., & Gorelick, S. M. (1994). Multiple-rate mass transfer for modeling diffusion and surface reactions in media with porescale heterogeneity. *Water Resources Research*, *31*(10), 2383–2400. https://doi.org/10.1029/95WR10583

Harvey, C., & Gorelick, S. M. (2000). Rate-limited mass transfer or macrodispersion: Which dominates plume evolution at the Macrodispersion Experiment (MADE) site? *Water Resources Research*, *36*(3), 637–650. https://doi.org/10.1029/1999WR900247

Harvey, C. F., Haggerty, R., & Gorelick, S. M. (1994). Aquifer remediation: A method for estimating mass transfer rate coefficients and an evaluation of pulsed pumping. *Water Resources Research*, *30*(7), 1979–1991. https://doi.org/10.1029/94WR00763

Huysmans, M., & Dassargues, A. (2005). *Review of the use of pé,clet numbers to determine the relative importance of advection and diffusion in low permeability environments*, *13*, 895–904.

Kang, P. K., Brown, S., & Juanes, R. (2016). Emergence of anomalous transport in stressed rough fractures. *Earth and Planetary Science Letters*, *454*, 46–54.

Kang, P. K., de Anna, P., Nunes, J. P., Bijeljic, B., Blunt, M. J., & Juanes, R. (2014). Pore-scale intermittent velocity structure underpinning anomalous transport through 3-d porous media. *Geophysical Research Letters*, *41*, 6184–6190. https://doi.org/10.1002/2014GL061475

Kang, P. K., Dentz, M., Le Borgne, T., & Juanes, R. (2011). Spatial Markov model of anomalous transport through random lattice networks. *Physical Review Letters*, *107*, 180602. https://doi.org/10.1103/PhysRevLett.107.180602

Kang, P. K., Le Borgne, T., Dentz, M., Bour, O., & Juanes, R. (2015). Impact of velocity correlation and distribution on transport in fractured media: Field evidence and theoretical model. *Water Resources Research*, *51*, 940–959. https://doi.org/10.1002/2014WR015799

Kowalczyk, P., Sprynskyy, M., Terzyk, A. P., Lebedynets, M., Namieśnik, J., & Buszewski, B. (2006). Porous structure of natural and modified clinoptilolites. *Journal of Colloid and Interface Science*, *297*(1), 77–85. https://doi.org/10.1016/j.jcis.2005.10.045

Le Borgne, T., Bolster, D., Dentz, M., de Anna, P., & Tartakovsky, A. M. (2011). Effective pore-scale dispersion upscaling with a correlated continuous time random walk approach. *Water Resources Research*, *47*, W12538. https://doi.org/10.1029/2011WR010457

Le Borgne, T., Dentz, M., & Carrera, J. (2008a). Spatial Markov processes for modeling Lagrangian particle dynamics in heterogeneous porous media. *Physical Review E*, *78*, 26308. https://doi.org/10.1103/PhysRevE.78.026308

Le Borgne, T., Dentz, M., & Carrera, J. (2008b). Lagrangian statistical model for transport in highly heterogeneous velocity fields. *Physical Review Letters*, *101*, 90601. https://doi.org/10.1103/PhysRevLett.101.090601

Major, E., Benson, D. A., Revielle, J., Ibrahim, H., Dean, A., Maxwell, R. M., et al. (2011). Comparison of Fickian and temporally non-local transport theories over many scales in an exhaustively sampled sandstone slab. *Water Resources Research*, *47*, W10519. https://doi.org/10.1029/2011WR010857

Matyka, M., Khalili, A., & Koza, Z. (2008). Tortuosity-porosity relation in porous media flow. *Physical Review E*, *78*, 26306. https://doi.org/10.1103/PhysRevE.78.026306

Morales, V. L., Dentz, M., Willmann, M., & Holzner, M. (2017). Stochastic dynamics of intermittent pore-scale particle motion in three-dimensional porous media: Experiments and theory. *Geophysical Research Letters*, *44*, 9361–9371. https://doi.org/10.1002/2017GL074326

National Research Council (2000). *Natural attenuation for groundwater remediation*. Washington, DC: Academic Press.

Reeves, D. M., Benson, D. A., & Meerschaert, M. M. (2008). Influence of fracture statistics on advective transport and implications for geologic repositories. *Water Resources Research*, *44*, W08405. https://doi.org/10.1029/2007WR006179

Sherman, T. (2018). Numerical implementation of the inverse spatial Markov model. Retrieved from https://github.com/tjsherman24/Inverse-Spatial-Markov

Sherman, T., Fakhari, A., Miller, S., Singha, K., & Bolster, D. (2017). Parameterizing the spatial Markov model from breakthrough curve data alone. *Water Resources Research*, *53*, 10,888–10,898. https://doi.org/10.1002/2017WR021810

Sprynskyy, M., Golembiewski, R., Trykowski, G., & Buszewski, B. (2010). Heterogeneity and hierarchy of clinoptilolite porosity. *Journal of Physics and Chemistry of Solids*, *71*(9), 1269–1277. https://doi.org/10.1016/j.jpcs.2010.05.006

St. Cloud Mining (2013). *NV-Na Ash Meadows clinoptilolite hydrous sodium aluminosilicate, natural cinoptilolite: Zeolite powders and granules PRODUCT DATA SHEET*. Winston: St. Cloud Mining, Product Data Sheet.

Sund, N. L., Bolster, D., & Benson, D. A. (2016). Testing the limits of the spatial Markov model for upscaling transport: The role of nonmonotonic effective velocity autocorrelations. *Physical Review E*, *94*(4), 43107.

Sund, N. L., Bolster, D., & Dawson, C. (2015). Upscaling transport of a reacting solute through a peridocially converging–diverging channel at pre-asymptotic times. *Journal of Contaminant Hydrology*, *182*, 1–15. https://doi.org/10.1016/j.jconhyd.2015.08.003

Sund, N., Bolster, D., Mattis, S., & Dawson, C. (2015). Pre-asymptotic transport upscaling in inertial and unsteady flows through porous media. *Transport in Porous Media*, *109*(2), 411–432.

Sund, N. L., Porta, G. M., & Bolster, D. (2017). Upscaling of dilution and mixing using a trajectory based spatial markov random walk model in a periodic flow domain. *Advances in Water Resources*, *103*, 76–85.

Sund, N., Porta, G., Bolster, D., & Parashar, R. (2017). A Lagrangian transport Eulerian reaction spatial (LATERS) Markov model for prediction of effective bimolecular reactive transport. *Water Resources Research*, *53*, 9040–9058. https://doi.org/10.1002/2017WR020821

Swanson, R. D., Binley, A., Keating, K., France, S., Osterman, G., Day-Lewis, F. D., & Singha, K. (2015). Anomalous solute transport in saturated porous media: Relating transport model parameters to electrical and nuclear magnetic resonance properties. *Water Resources Research*, *51*, 1264–1283. https://doi.org/10.1002/2014WR015284

Swanson, R. D., Singha, K., Day-Lewis, F. D., Binley, A., Keating, K., & Haggerty, R. (2012). Direct geoelectrical evidence of mass transfer at the laboratory scale. *Water Resources Research*, *48*, W10543. https://doi.org/10.1029/2012WR012431

Willmann, M., Carrera, J., & Sánchez-Vila, X. (2008). Transport upscaling in heterogeneous aquifers: What physical parameters control memory functions? *Water Resources Research*, *44*, W12437. https://doi.org/10.1029/2007WR006531

Yuan-Hui, L., & Gregory, S. (1974). Diffusion of ions in sea water and in deep-sea sediments. *Geochimica et Cosmochimica Acta*, *38*(5), 703–714.

Zhang, Y., Benson, D. A., Meerschaert, M. M., & LaBolle, E. M. (2007). Space-fractional advection-dispersion equations with variable parameters: Diverse formulas, numerical solutions, and application to the Macrodispersion Experiment site data. *Water Resources Research*, *43*, W05439. https://doi.org/10.1029/2006WR004912

Zhang, Y., Benson, D. A., & Reeves, D. M. (2009). Time and space nonlocalities underlying fractional-derivative models: Distinction and literature review of field applications. *Advances in Water Resources*, *32*(4), 561–581. https://doi.org/10.1016/j.advwatres.2009.01.008

Zinn, B., & Harvey, C. F. (2003). When good statistical models of aquifer heterogeneity go bad: A comparison of flow, dispersion, and mass transfer in connected and multivariate gaussian hydraulic conductivity fields. *Water Resources Research*, *39*(3), 1051. https://doi.org/10.1029/2001WR001146